ACS APPLIED MATERIALS & INTERFACES

Research Article

www.acsami.org

TiO_2 Nanorods: A Facile Size- and Shape-Tunable Synthesis and Effective Improvement of Charge Collection Kinetics for Dye-Sensitized Solar Cells

Wenjun Zhang,[†,‡] Yan Xie,[†,‡] Dehua Xiong,[†] Xianwei Zeng,[†] Zhihong Li,[†] Mingkui Wang,[†] Yi-Bing Cheng,[†] Wei Chen,*[,†] Keyou Yan,[§] and Shihe Yang*[,§]

[†]Michael Gratzel Center for Mesoscopic Solar Cells, Wuhan National Laboratory for Optoelectronics, Huazhong University of Science and Technology, Wuhan, China

[§]Department of Chemistry, The Hong Kong University of Science and Technology, Clear Water Bay, Kowloon, Hong Kong

Supporting Information

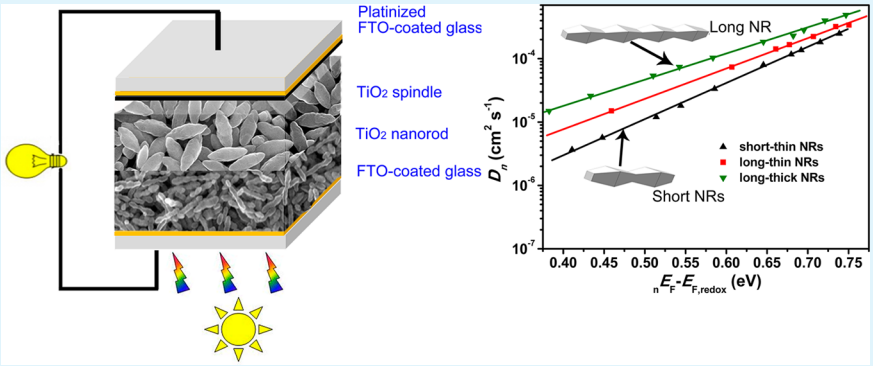

ABSTRACT: In this paper, we present a novel, high-yield, and cost-effective hydrothermal method for the preparation of single crystal-like anatase TiO_2 nanorods (NRs) with specific {101} exposed crystal planes and preferred [001] growth direction, which is governed by the "oriented attachment" mechanism. The successful synthesis of TiO_2 NRs and fine tuning on their size and shape could be easily accomplished by adjusting the solvent compositions. The salient feature of these NRs, in lieu of traditional nanoparticles as building blocks of photoanodes in dye-sensitized solar cell (DSSC) system, rests with their significantly reduced grain boundaries. The electron diffusion and recombination kinetics have been critically compared for the first time with respect to the size and shape of the novel building blocks. A high efficiency of 8.87% has finally been achieved for DSSC based on long-thin NRs rather than short-thin or long-thick NRs, which possesses balanced optimizations on charge collection and light-harvesting properties.

KEYWORDS: *TiO_2 nanorod, oriented attachment, anatase, dye-sensitized, solar cell*

INTRODUCTION

TiO_2 is one of the most successful materials widely explored and used in solar cells,[1−3] photocatalysis,[4,5] lithium batteries,[6] photochromic devices,[7,8] etc., because of its unique chemical, electrical and optical properties. Despite the voluminous reports on the synthesis of nanosized TiO_2 over the last two decades,[9] major challenges remain on precise control over the nanometric size, shape, and surface structure in a simple and easily scalable fashion.[10−12] Yet understanding the size-, shape-, and/or surface-dependent properties of nanosized TiO_2 lies at the heart of developing high-performance devices.[12−14]

As a core photoanode material of dye-sensitized solar cell (DSSC), a technically and economically credible alternative to the currently dominating p−n junction photovoltaic devices, TiO_2 needs to be highly crystalline but nanoporous with high surface area and high connectivity so that sufficient dye molecules can be adsorbed and plenty of photoelectrons can be quickly injected and extracted to external circuit.[15,16] Charge collection efficiency of the photoanode is dictated by the kinetic competition between electron transport in nanocrystalline TiO_2 film and recombination at the TiO_2/electrolyte interface, which historically has been optimized regarding the nanoparticle (NP) size, network geometry, etc.[17−20] In the current "record" cells, the charge collection loss during electron diffusion is generally considered to be small or negligible.[15,21] For example, by electrochemical impedance spectroscopy analysis, Gratzel and co-workers claimed that the effective diffusion length in efficient DSSC was >50 μm, 2−3 times that of the actual film thickness (5-16 μm), implying only <2% collection loss of the injected electrons.[21] Recently, however, O'regan et al.

Received: April 8, 2014
Accepted: May 15, 2014
Published: May 15, 2014

argued that the effective diffusion length measured by standard dynamic techniques was largely overestimated. They revised the value through steady-state spectral response measurements to about 10−20 μm, very comparable to the actual film thickness.[22] Notwithstanding such unsettled debate, it is reasonable that high densities of grain boundaries and surface defects, associated with the traditional NP films, would hinder fast electron transport and cause considerable interfacial recombination, as have been experimentally demonstrated.[16] To resolve this problem, one-dimensional (1D) nanoarrays, such as ZnO nanowires,[23] TiO_2 nanowires/nanotubes,[24,25] etc., have been explored as they were suggested to have ideal boundary-free electron transport paths. Indeed, the nanoarrays have exhibited much faster electron transport and/or longer electron lifetime than the NP counterparts. Unfortunately, performance of such nanoarray-based DSSCs still lags much behind because of insufficient dye adsorption due to low surface area, inadequate charge collection due to poor surface structure, and adverse light scattering due to unoptimized 3D structure.[25] Adding to the problem is the practical difficulty for large-scale production of such nanoarrays. Hence, it is still a significant goal to synthesize size/shape-tunable, surface-controllable and highly dispersible nanorods (NRs) or nanowires (NWs) as alternative to the 20 nm TiO_2 NPs for DSSCs, by using technology that is compatible with fast screen printing technique.[26] We notice that randomly assembled TiO_2 NRs/nanowires have been exploited in DSSC system very early on which inspired numerous fololow-up studies,[27−31] but the question about how tiny changes in the 1D nanomaterial's size and shape parameters affect the charge collection kinetics and the solar cell performance are still not clear.

In this paper, we present a novel, high-yield, and cost-effective hydrothermal method for preparing single crystalline anatase TiO_2 NRs laterally bounded by the {101} crystal planes and preferentially grown in the [001] direction, which was achieved by taking advantage of an "oriented attachment" mechanism. Though, similar morphologies have been reported in the literature variously,[29,30,32,33] several differences of our strategy from others are noteworthy: (1) the whole oriented attachment process was accomplished by a one-pot hydrothermal reaction in one run, (2) the process avoided using expensive solvents or additives, (3) size parameters of the NRs could be finely tuned in the range of 15-25 nm (diameter) × 50−150 nm (length), very suitable for high-performance DSSCs, (4) the NRs are highly dispersible unlike aggregates reported previously which may make it difficult to fully excavate the NRs' potential. The successful synthesis of TiO_2 NRs with tunable diameter and aspect ratio, easily accomplished with our strategy by adjusting the solvent compositions, has allowed us for the first time to conduct comparative studies with nanorods of different size/shape/surface parameters and thereby optimize cell performance while monitoring their charge collection kinetics.

RESULTS AND DISCUSSION

Three kinds of NRs were chosen for our study as DSSC photoanodes: "short-thin NRs" with a mean diameter of 15 nm and length of 50 nm (Figure 1a, see Figure S1 in the Supporting Information), "long-thin NRs" with a mean diameter of 17 nm and length of 120 nm (Figure 1b), "long-thick NRs" with a mean diameter of 25 nm and length of 150 nm (Figure 1c). Scanning electron microscopy (SEM) images (Figure 1a−c) clearly reveal the uniform and well-defined

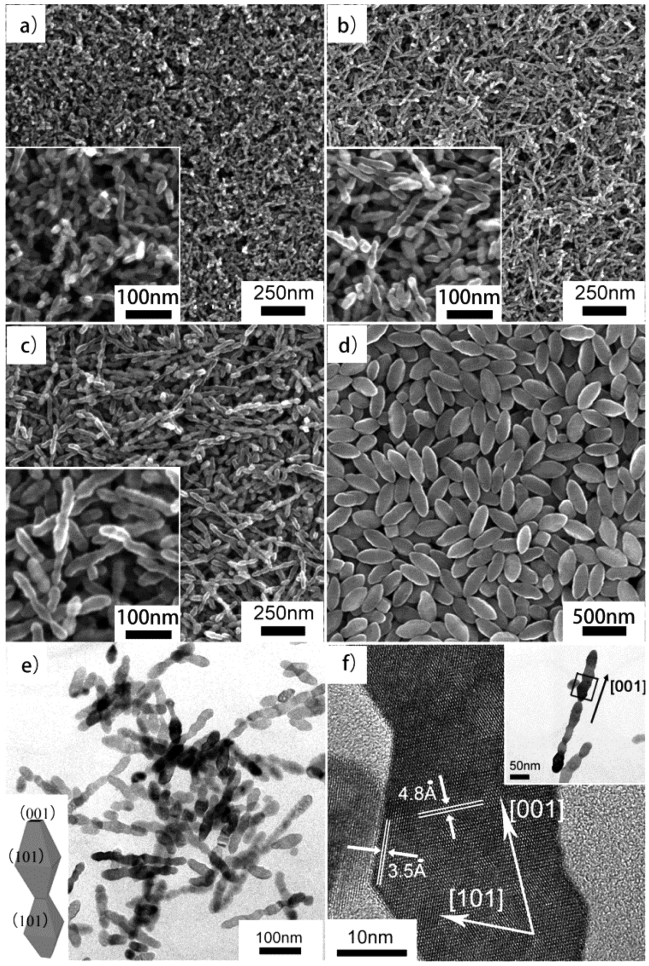

Figure 1. SEM images of three kinds of TiO_2 NRs: (a) short-thin NRs (15 × 50 nm); (b) long-thin NRs (17 × 120 nm); and (c) thick-long NRs (25 × 150 nm). (d) SEM image of 200 × 450 nm large spindle-like particles. The insets to a−c are the corresponding blown-up images. (e) TEM image and (f) high-resolution TEM image of the NRs in (c); the measured lattice parameters are consistent with the exposed crystal side-surfaces all being the {101} planes of anatase and the anisotropic oriented attachment growth direction being [001]. An ideal oriented attachment NR is schematically shown in the inset of e.

morphologies of the as-synthesized TiO_2 NRs with different diameters and lengths as described above. The NRs are observed to have folded outer crystal surface, a typical feature of NRs formed by "oriented attachment".[33,34] The morphology implies incomplete fusion at the necks between primary crystallites, distinct from the traditional "Oswald ripening" related growth, in which smaller particles are generally all exhausted to promote the growth of bigger ones.[35] As confirmed by transmission electron microscopy (TEM) images (Figure 1e, f, and Figure S1 in the Supporting Information), the NRs are well-dispersed without aggregation and each of the NRs is made from several primary crystallites with the typical shape of anatase tetragonal {101} bipyramids, which are interconnected through the (001) surface. "short-thin" NRs are generally formed by attachment of 2−3 bipyramids (Figure S1 in the Supporting Information), whereas "long-thick" NRs are connected by 4-7 primary crystallites (Figure 1e). According to the typical theoretical explanation, the driving force for such oriented attachment process is to minimize the total surface energy of the reaction system.[35] Because the {001} crystal

dx.doi.org/10.1021/am502067r | ACS Appl. Mater. Interfaces 2014, 6, 9698−9704

planes of anatase are of higher surface energy than the {101} planes by ~25%,[10,11] it is reasonable that the oriented attachment occurs preferentially along the [001] direction to minimize the exposed {001} surfaces. In our strategy, ethylene glycol in the composite solvent has proved critical in promoting such an oriented attachment process. As can be seen clearly from Figure S2 in the Supporting Information, only when a certain volume ratio of ethylene glycol was contained in the composite solvent, oriented attachment could occur. The inherent reason should be ascribed to the strong chelation of ethylene glycol to Ti centres. Direct evidence is that for the as-synthesized products from ethylene glycol containing hydrothermal conditions, though after thorough washing, the peaks representing the existence of surface absorbed ethylene glycol molecules are present in all of their FTIR spectra (see Figure S3 in theSupporting Information). Perhaps, ethylene glycol molecules possess different absorption affinity on different crystal planes of primary anatase crystallites, making the energy difference between {101} and {001} planes even larger than no ethylene glycol mediated samples, and therefore promote the anisotropic assembly through the active {001} planes.[36] Careful tuning of the composition ratios of ethanol, water and ethylene glycol in the solvent (see Experiment Sectional and Table S1 in the Supporting Information) may affect their adsorbing state onto different crystal planes of anatase primary crystallites, changing their surface energetic differences. As a result, the crystal growth and oriented attachment rates in certain directions can be adjusted. All of these provide the oriented attachment for the formation of NRs in a controllable manner, leading to three kinds of NRs as shown in Figure 1, which provide an ideal material base for comparative study of the size/shape-perfromance relationship in DSSCs. X-ray diffraction (XRD) patterns (see Figure S4 in the Supporting Information) confirm that the three kinds of NRs are all in pure anatase crystal phase and their anisotropic crystal growth directions are [001]. The average diameters of three kind NRs are calculated to be 15.0, 16.8, 25.2 nm respectively, by applying the Scherrer equation to the broadened (200) diffraction peaks, which are consistent with SEM and TEM observations. Shown in Figure 1d are uniform spindlelike anatase TiO_2 particles with the size of about 200 × 450 nm (corresponding XRD pattern is shown in Figure S4 in the Supporting Information), synthesized in a similar hydrothermal condition to NRs but with a decreased concentration of the Ti source and an increased alkaline concentration. Those two changes in synthesis condition led to fewer crystal seeds and higher condensation reaction rate, giving rise to the growth of bigger particles, which are ideal for constructing a light-scattering layer of DSSCs.

It is known that light scattering could enhance light harvesting of DSSCs, especially in the spectral region where dye absorbs weakly, and ~15% improvement brought about this way in solar cell performance has been reported.[37] In general, it can be realized by employing a double-layered structure design of photoanode: a transparent underlayer consisting of small building blocks providing huge surface area for sufficient dye adsorbing, while a toplayer made of big particles can reflect the partially transmitted light back to be absorbed again by the underlayer.[38] As reflected by the diffuse reflectance spectrum shown in Figure S5 in the Supporting Information, a 6 μm thick film made of our large spindlelike particles could reflect 70−90% fraction of solar light back, which attests its strong enough scattering capability. DSSCs using such kind of 6 μm thick film as light scattering layer and the three kinds of NR films with thickness of about 10 ± 0.5 μm as the underlayers were then subjected to device measurements.

From Figure 2a, the long-thin NR based photoanode shows a short-circuit current density (J_{sc}) of 17.4 mA cm^{-2}, open-circuit

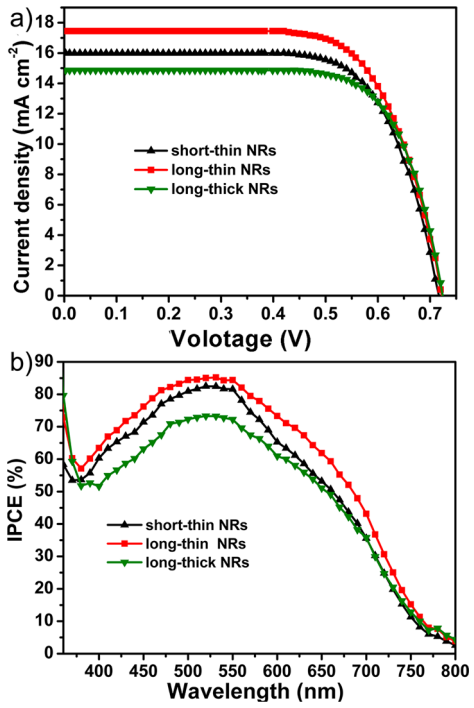

Figure 2. (a) $J-V$ characteristic curves of DSSCs based on the three TiO_2 NRs photoanodes under AM 1.5 simulated sunlight with a power density of 100 mW cm^{-2}. (b) IPCE spectra of the three different DSSC devices.

voltage (V_{oc}) of 721.2 mV, fill factor (FF) of 0.71, and therefore an overall energy-conversion efficiency (η) of 8.87%, which is much improved than that of the short-thin and long-thick NRs based photoanodes with moderate η of 8.09% and 7.81%, respectively (Table 1). The improvement on η mostly rests with the higher J_{sc} of the former sample than the latter two (17.4 mA cm^{-2} versus 16.0 and 14.9 mA cm^{-2}, Table 1). The inherent reasons for J_{sc} improvements will be elucidated in terms of the determining factors of IPCE, including light harvesting efficiency (LHE), charge injection efficiency (Φ_{inj}), and charge collection efficiency (η_{cc}), according to the equation of IPCE = LHE$\Phi_{inj}\eta_{cc}^2$.

First of all, Φ_{inj} can be neglected, which is generally very close to 100% in case of efficient ruthlium dye (like the Z907 dye used in this work) sensitized onto TiO_2.[39] With respect to LHE, it is primarily determined by the Beer's law via the equation,[40] LHE(λ) = 1 − $10^{-\Gamma\times\sigma(\lambda)}$, where Γ is concentration of dye adsorbed on TiO_2 surface (here determined to be 1.43 × 10^{-7}, 1.32 × 10^{-7}, 0.73 × 10^{-7} mol cm^{-2} for three kinds of photoanodes, respectively, which are nearly proportional to their BET surface areas, as listed in Table 1) and σ is the absorption cross section of Z907 dye (σ = 1.22 × 10^7 cm^2 mol^{-1} at 540 nm).[41] Accordingly, $LHE_{(540\ nm)}$ are calculated to be 98.2%, 97.5%, and 87.1% for short-thin, long-thin and long-thick NR based films, respectively. The LHE for the short-thin NR based film is slightly larger than the long-thin NR based film. However, the superior LHE of short-thin NR does not lead to a higher IPCE than the long-thin NR based film (Figure

dx.doi.org/10.1021/am502067r | ACS Appl. Mater. Interfaces 2014, 6, 9698−9704

Table 1. Performance Parameters of DSSCs Based on Photoanodes Made of Different TiO_2 NRs

samples	V_{oc} (mV)	J_{sc} (mA cm^{-2})	FF	η (%)	surface area (m^2 g^{-1})	absorbed dye ($\times 10^{-7}$ mol cm^{-2})	IPCE maximum at 540 nm (%)
short-thin	716.9	16.0	0.71	8.09	105.5	1.43	81.7
long-thin	721.2	17.4	0.71	8.87	104.8	1.32	84.3
long-thick	723.9	14.9	0.73	7.81	50.0	0.73	72.7

2b). From such an inconsistence, there should be another factor effect on IPCE. We then turn to the charge collection efficiency η_{cc}.

Charge collection efficiency η_{cc} is determined by the kinetic competition between electron transport and interfacial recombination. In order to evaluate how the size and shape of NRs affect the competing kinetics and clarify the inherent relationship between the cell performance and the NRs' morphology, photocurrent/photovoltage transient decay techniques were employed to measure the electron transport time (τ) and recombination time (τ_r, also called lifetime).[42] The operating principles and the experimental conditions for these measurements are described in the Supporting Information (Figure S6). By varying the incident light intensity, the voltage of the cell, or more accurately the quasi Femi level or the electron density of the film is accordingly tuned, τ and τ_r at different voltages can be obtained by fitting the photocurrent and photovoltage decay curves, respectively. The voltage is equal to the offset of the electron quasi Fermi level of TiO_2 with respect to the redox electrolyte, denoted as "$_nE_F - E_{F,\,redox}$". Taking note that the film thickness, d, has effects on τ, we chose electron diffusion coefficient ($D_n = d^2/2.35\tau$)[43] instead of τ to more accurately evaluate the photoanode films' electron transport kinetics. From Figure 3b, c, it is clear that (1) the dependences of D_n and τ_r on "$_nE_F - E_{F,\,redox}$" fit well with the power law; (2) with the increasing "$_nE_F - E_{F,\,redox}$" value, D_n monotonically increases and τ_r monotonically decreases. These phenomena are all in accordance with the well-known multiple trapping model.[44,45] In this model, electrons perform a random walk between trap sites, the location of which can be described by an exponential distribution function, which is the origin of the observed power law dependences.[19] With the increasing "$_nE_F - E_{F,\,redox}$", corresponding to electrons at the quasi-Femi level closer to the conduction band edge, the electrons require a smaller activation energy or a shorter waiting time to be detrapped, which is why the corresponding D_n is larger; by the same token, it becomes easier for the electrons to migrate to the TiO_2/electrolyte interface leading to the corresponding shorter τ_r.

In more detail, from Figure 3b, D_n of the three kind photoanodes are found in the sequence of long-thick NRs > long-thin NRs > short-thin NRs in the whole tested range of "$_nE_F - E_{F,\,redox}$". From the above sequence, it appears that the longer NRs formed by oriented attachment of more primary crystallites, meaning a smaller grain boundary density when forming a porous film, always correspond to a higher D_n. As illustrated in Figure 3a, "short NRs" consisting of two primary crystallites would lead to a porous film possessing twice the grain boundary density of that with "long NRs" obtained by oriented attachment from four primary crystallites. Traps located at the crystal surface were also suggested to be involved in electron transport.[46] A higher surface area then corresponds to a higher density of surface traps and therefore a lower D_n.[18,47] Perhaps, this can partially explain why D_n of long-thick NR-based film is relatively higher than that of long-thin NR-based film, considering that the BET surface area of the former is nearly twice lower than the latter.

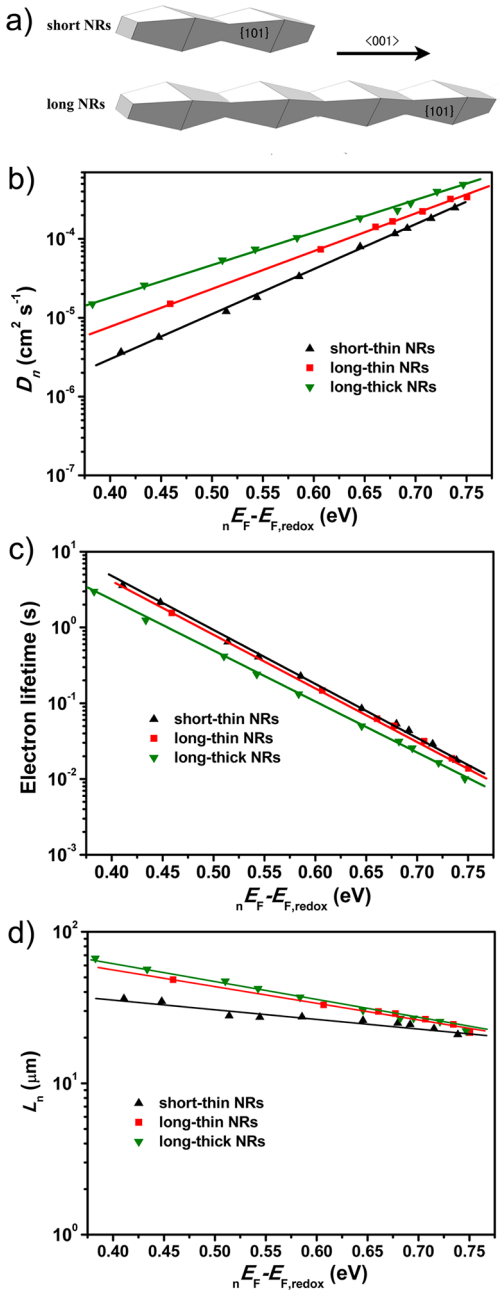

Figure 3. (a) Anatase crystal growth modes of NRs; comparisons of (b) electron diffusion coefficient, D_n, (c) electron lifetime, τ_r, and (d) electron diffusion length, L_n, as a function of the offset of the electron quasi Fermi level of TiO_2 with respect to the redox electrolyte, $_nE_F - E_{F,redox}$, between the three kind photoanodes based on short-thin, long-thin, and long-thick NRs. $_nE_F - E_{F,redox}$ is equal to the measured open circuit voltage of the cells under different light intensities. The straight lines represent the power-law fitting.

dx.doi.org/10.1021/am502067r | ACS Appl. Mater. Interfaces 2014, 6, 9698−9704

In contrast to evidently different D_n for the three kind films, their τ_r measured are much more comparable (Figure 3c). τ_r of long-thick NR based film is slightly shorter than that of the other two NRs based films, which is opposite to their D_n sequence. A reasonable explanation is that recombination is transport limited in porous films. Namely, with faster diffusion, there is a greater probability per unit time that electrons encounter relatively "rare" and stationary I_2 recombination sites, which would in turn lead to faster recombination.[48]

Combining D_n together with τ_r allows us to weigh the charge collection property of the three kind films on the basis of their effective electron diffusion length (L_n), by using the equation $L_n = (D_n\tau_r)^{-1/2}$ for calculation.[20] L_n rather than individual D_n or τ_r is the direct parameter closely related to charge collection efficiency η_{cc} of the photoanode film. From Figure 3d, L_n of the three kind films, or to say their η_{cc} are in the sequence of long-thick NR ≥ long-thin NR > short-thin NR, which is basically in accordance with their D_n sequence.

By comprehensive review of *LHE* and η_{cc} sequences for the three kind films, there is no doubt on the IPCE sequence of long-thin NR > short-thin NR-based film. Only question left over is that *IPCE* of long-thick NR-based film is not as-predicted by its η_{cc} position. It should be because of its evidently lower dye adsorbing amount, and therefore shortage on LHE plays the dominate role than η_{cc} in determining its IPCE maximum at 540 nm. Actually, this shortage could be compensated partially at the longer wavelength region of 600−750 nm because of its stronger light scattering ability, as reflected by their diffuse reflectance spectra in Figure S5 in the Supporting Inforation. The wider pore size distribution of long-thick NR-based film (see Figure S7 in the Supporting Information) holds the key for its stronger light scattering ability than the other two kinds of NRs.

CONCLUSION

In summary, we have reported a novel and facile hydrothermal process for fabricating size and shape controllable anatase TiO_2 NRs governed by the "oriented attachment" mechanism. The NRs have a high surface area desirable for large amounts of dye adsorption, and when used together with a light scattering layer made of large spindlelike particles synthesized in a similar hydrothermal condition for DSSC photoanodes, they ensure excellent light harvesting. The single-crystalline longer TiO_2 NRs have much decreased grain boundaries compared to shorter NRs, giving rise to higher charge collection efficiency. On balance between the optimizations of light-harvesting and charge collection efficiencies, the long-thin NR based film has demonstrated the highest efficiency at 8.87%. More important, the excellent charge collection property and the wide pore size tunability could be simultaneously realized in the NR-based photoanodes. Those characteristics are both in critical need for various photoelectrochemical applications. Related studies to further exploit the potential of the "oriented attachment" NRs in various directions are on-going in our laboratories.

EXPERIMENTAL SECTION

Synthesis of NRs and Large Spindlelike Particles. All solvent and reagents were of analytical pure grade quality and were used as-received. In a typical synthesis, tetramethylammonium hydroxide solution (25 wt % in water), ethanol and distilled water were first added to a 100 mL round bottom flask. Then, a mixture of ethylene glycol and titanium isopropoxide was dropwise added to above solution with vigorous stirring at 80 °C until a transparent solution was obtained. Afterward, the mixture was then transferred into a Teflon autoclave with a capacity of 100 mL and kept at 230 °C for 24 h. After the autoclave was cooled to room temperature naturally, a white product was collected by successive centrifugation and washing with ethanol for several times. The diameter and length of NRs can be facilely controlled by changing the composition of precursors, so as to large spindlelike particles (see Table S1 in the Supporting Information).

Fabrication of TiO_2 Photoanode Films and DSSC. Homogenous screen printing pastes were made strictly according to the reference.[37] Films were fabricated on a conducting substrates (FTO-coated glass, 8 Ω/square, Nippon Sheet Glass, Japan) by screen printing. The freshly deposited films were gradually heated at 325°C for 5 min, at 375°C for 5 min, at 450°C for 15 min, and finally, at 500°C for 15 min. The sintered films were then treated in 40 mM aquestion solution of $TiCl_4$ at 70°C for 30 min and calcined at 500°C for 30 min again. After cooling to 80°C, the TiO_2 films were immersed in 0.3 mM Z907 dye solution with 3-phenylpropionic acid (300 mM) as coadsorbent in a mixture of acetonitrile and *tert*-butyl alcohol (1/1, v/v) for 16 h. After rinsing in acetonitrile, the TiO_2 electrodes were assembled with thermally platinized conductive counter electrode. The two plates were sandwiched together with hot melt polymer gasket (Surlyn, 25 μm). The electrolyte consisting of 1.0 mM 1,3-dimethylimidazolium iodide, 50 mM LiI, 30 mM I_2 in a mixture of acetonitrile, and valeronitrile (85/15, v/v) was introduced through a small hole drilled in the counter electrode via vacuum backfilling.

Characterizations. Morphologies of the nanomaterials were characterized by SEM (FEI Sirion 200) at an accelerating voltage of 10 kV. TEM observations were carried out on a JEOL 2010F microscope operating at 200 kV. XRD patterns of the TiO_2 powders were obtained with a PANalytical B.V. X-ray diffraction system. Diffuse-reflectance spectra were measured on a PerkinElmer UV/Vis spectrophotometer (model Lambda 950). BET surface areas and pore size distributions of the film samples were characterized by using a ASAP 2020 accelerated surface area and porosimetry system. Dye adsorption amount was determined by immersing the films in 1 mM NaOH solution and monitoring the concentration of desorbed dye. The film thickness was determined by a Veeco Dektak 150 surface profiler system. The photocurrent-voltage characteristics were measured using a Newport AM 1.5 solar simulator (model 91192) at the light intensity of 100 mW cm^{-2}, calibrated by a standard silicon reference cell. IPCE was measured on the basis of a Newport Apex Monochromator illuminator (model 70104). Photocurrent/photovoltage transient decays were measured on a home-made photoelectrical system, more details could be found in the Supporting Information.

ASSOCIATED CONTENT

Supporting Information

TEM images of short-thin NRs with the size of about 15 × 50 nm, FT-IR spectra of different produtcs prepared from varied hydrothermal precursors, SEM image of products synthesized in similar hydrothermal conditions by varing the volume ratios of EG and distill water as the solvents, XRD patterns of the as-prepared films made of different NRs and large spindlelike particles, diffuse reflectance spectra of the films made of three kinds of NRs, details of transient photovoltage decay and transient photocurrent measurement, pore size distributions of the films made of three kinds of NRs, the ratios of reagents in the hydrothermal precursors for the synthesis of different NRs and large spindlelike particles. This material is available free of charge via the Internet at http://pubs.acs.org.

AUTHOR INFORMATION

Corresponding Authors

*E-mail: wnlochenwei@mail.hust.edu.cn.
*E-mail: chsyang@ust.hk

Author Contributions

‡Authors W.Z. and Y.X. contributed equally to this paper.

Notes

The authors declare no competing financial interest.

■ ACKNOWLEDGMENTS

This work was supported by National Natural Science Foundation (21103058, 21173091, 20903030), 973 Program of China (2011CBA00703), and Basic Scientific Research Funds for Central Colleges (2012YQ027, 2013TS040). We thank Analytical and Testing Center of Huazhong University Science & Technology for the sample measurements.

■ REFERENCES

(1) O'Regan, B.; Grätzel, M. A Low-Cost, High-Efficiency Solar Cell Based on Dye-sensitized Colloidal TiO_2 Films. *Nature* **1991**, *353*, 737−740.

(2) Yella, A.; Lee, H. W.; Tsao, H. N.; Yi, C.; Chandiran, A. K.; Nazeeruddin, M. K.; Diau, E. W. G.; Yeh, C. Y.; Zakeeruddin, S. M.; Grätzel, M. Porphyrin-Sensitized Solar Cells with Cobalt f(II/III)-Based Redox Electrolyte Exceed 12 Percent Efficiency. *Science* **2011**, *334*, 629−634.

(3) Pattantyus-Abraham, A. G.; Kramer, I. J.; Barkhouse, A. R.; Wang, X. H.; Konstantatos, G.; Debnath, R.; Levina, L.; Raabe, I.; Nazeeruddin, M. K.; Grätzel, M.; Sargent, E. H. Depleted-Heterojunction Colloidal Quantum Dot Solar Cells. *ACS Nano* **2010**, *4*, 3374−3380.

(4) Wang, R.; Hashimoto, K.; Fujishima, A.; Chikuni, M.; Kojima, E.; Kitamura, A.; Shimohigoshi, M.; Watanabe, T. Light-Induced Amphiphilic Surfaces. *Nature* **1997**, *388*, 431−432.

(5) Chen, X. B.; Liu, L.; Yu, P. Y.; Mao, S. S. Increasing Solar Absorption for Photocatalysis with Black Hydrogenated Titanium Dioxide Nanocrystals. *Science* **2011**, *331*, 746−750.

(6) Wagemaker, M.; Kentgens, A. P. M.; Mulder, F. M. Equilibrium Lithium Transport between Nanocrystalline Phases in Intercalated TiO_2 Anatase. *Nature* **2002**, *418*, 397−399.

(7) Naoi, K.; Ohko, Y.; Tatsuma, T. TiO_2 Films Loaded with Silver Nanoparticles: Control of Multicolor Photochromic Behavior. *J. Am. Ceram. Soc.* **2004**, *126*, 3664−3668.

(8) Ohko, Y.; Tatsuma, T.; Fujii, T.; Naoi, K.; Niwa, C.; Kubota, Y.; Fujishima, A. Multicolour Photochromism of TiO_2 Films Loaded with Silver Nanoparticles. *Nature Materials* **2002**, *2*, 29−31.

(9) Chen, X.; Mao, S. S. Titanium Dioxide Nanomaterials: Synthesis, Properties, Modifications, and Applications. *Chem. Rev.* **2007**, *107*, 2891−2959.

(10) Yang, H. G.; Sun, C. H.; Qiao, S. Z.; Zou, J.; Liu, G.; Smith, S. C.; Cheng, H. M.; Lu, G. Q. Anatase TiO_2 Single Crystals With a Large Percentage of Reactive Facets. *Nature* **2008**, *453*, 634−638.

(11) Barnard, A. S.; Curtiss, L. A. Prediction of TiO_2 Nanoparticle Phase and Shape Transitions Controlled by Surface Chemistry. *Nano Lett.* **2005**, *5*, 1261−1266.

(12) Qiu, Y. C.; Chen, W.; Yang, S. H. Double-Layered Photoanodes from Variable-Size Anatase TiO_2 Nanospindles: A Candidate for High-Efficiency Dye-Sensitized Solar Cells. *Angew. Chem., Int. Ed.* **2010**, *49*, 3675−3679.

(13) D'Arienzo, M.; Carbajo, J.; Bahamonde, A.; Crippa, M.; Polizzi, S.; Scotti, R.; Wahba, L.; Morazzoni, F. Photogenerated Defects in Shape-Controlled TiO_2 Anatase Nanocrystals: A Probe to Evaluate the Role of Crystal Facets in Photocatalytic Processes. *J. Am. Chem. Soc.* **2011**, *133*, 17652−17661.

(14) Tachikawa, T.; Yamashita, S.; Majima, T. Evidence for Crystal-Face-Dependent TiO_2 Photocatalysis from Single-Molecule Imaging and Kinetic Analysis. *J. Am. Chem. Soc.* **2011**, *133*, 7197−7204.

(15) Tetreault, N.; Grätzel, M. Novel Nanostructures for Next Generation Dye-Sensitized Solar Cells. *Energy. Environ. Sci.* **2012**, *5*, 8506−8516.

(16) Martinson, A. B. F.; Hamann, T. W.; Pellin, M. J.; Hupp, J. T. New Architectures for Dye-Senstized Solar Cells. *Chem. Eur. J.* **2008**, *14*, 4458−4467.

(17) Cass, M. J.; Qiu, F. L.; Walker, A. B.; Fisher, A. C.; Peter, L. M. Influence of Grain Morphology on Electron Transport in Dye Sensitized Nanocrystalline Solar Cells. *J. Phys. Chem. B* **2003**, *107*, 113−119.

(18) Nakade, S.; Saito, Y.; Kubo, W.; Kitamura, T.; Wada, Y.; Yanagida, S. Influence of TiO_2 Nanoparticle Size on Electron Diffusion and Recombination in Dye-Sensitized TiO_2 Solar Cells. *J. Phys. Chem. B* **2003**, *107*, 8607−8611.

(19) J. Frank, A.; Kopidakis, N.; Lagemaat, J. v. d. Electrons in Nanostructured TiO_2 Solar Cells: Transport, Recombination and Photovoltaic Properties. *Coord. Chem. Rev.* **2004**, *248*, 1165−1179.

(20) Oekermann, T.; Zhang, D.; Yoshida, T.; Minoura, H. Electron Transport and Back Reaction in Nanocrystalline TiO_2 Films Prepared by Hydrothermal Crystallization. *J. Phys. Chem. B* **2004**, *108*, 2227−2235.

(21) Wang, Q.; Ito, S.; Grätzel, M.; Fabregat-Santiago, F.; Mora-Sero, I.; Bisquert, J.; Bessho, T.; Imai, H. Characteristics of High Efficiency Dye-Sensitized Solar Cells. *J. Phys. Chem. B* **2006**, *110*, 25210−25221.

(22) Barnes, P. R. F.; Liu, L.; Li, X.; Anderson, A. Y.; Kisserwan, H.; Ghaddar, T. H.; Durrant, J. R.; O'Regan, B. C. Re-evaluation of Recombination Losses in Dye-Sensitized Cells: The Failure of Dynamic Relaxation Methods to Correctly Predict Diffusion Length in Nanoporous Photoelectrodes. *Nano Lett.* **2009**, *9*, 3532−3538.

(23) Law, M.; Greene, L. E.; Johnson, J. C.; Saykally, R.; Yang, P. Nanowire Dye-Sensitized Solar Cells. *Nature Materials* **2005**, *4*, 455−459.

(24) Feng, X. J.; Shankar, K.; Varghese, O. K.; Paulose, M.; Latempa, T. J.; Grimes, C. A. Vertically Aligned Single Crystal TiO_2 Nanowire Arrays Grown Directly on Transparent Conducting Oxide Coated Glass: Synthesis Details and Applications. *Nano Lett.* **2008**, *8*, 3781−3786.

(25) Varghese, O. K.; Paulose, M.; Grimes, C. A. Long Vertically Aligned Titania Nanotubes on Transparent Conducting Oxide for Highly Efficient Solar Cells. *Nat. Nanotechnol.* **2009**, *4*, 592−597.

(26) Tetreault, N.; Horvath, E.; Moehl, T.; Brillet, J.; Smajda, R.; Bungener, S.; Cai, N.; Wang, P.; Zakeeruddin, S. M.; Forro, L.; Magrez, A.; Grätzel, M. High-Efficiency Solid-State Dye-Sensitized Solar Cells: Fast Charge Extraction through Self-Assembled 3D Fibrous Network of Crystalline TiO_2 Nanowires. *ACS Nano* **2010**, *4*, 7644−7650.

(27) De Marco, L.; Manca, M.; Giannuzzi, R.; Malara, F.; Melcarne, G.; Ciccarella, G.; Zama, I.; Cingolani, R.; Gigli, G. Novel Preparation Method of TiO_2-Nanorod-Based Photoelectrodes for Dye-Sensitized Solar Cells with Improved Light-Harvesting Efficiency. *J. Phys. Chem. C* **2010**, *114*, 4228−4236.

(28) Jiu, J. T.; Isoda, S.; Wang, F. M.; Adachi, M. Dye-sensitized Solar Cells Based on a Single-Crystalline TiO_2 Nanorod Film. *J. Phys. Chem. B* **2006**, *110*, 2087−2092.

(29) Adachi, M.; Murata, Y.; Takao, J.; Jiu, J. T.; Sakamoto, M.; Wang, F. M. Highly efficient Dye-Sensitized Solar Cells with a Titania Thin-Film Electrode Composed of a Network Structure of Single-Crystal-Like TiO_2 Nanowires Made by the "Oriented Attachment" Mechanism. *J. Am. Chem. Soc.* **2004**, *126*, 14943−14949.

(30) Buonsanti, R.; Carlino, E.; Giannini, C.; Atamura, D.; De Marco, L.; Giannuzzi, R.; Manca, M.; Gigli, G.; Cozzoli, P. D. Hyperbranched Anatase TiO_2 Nanocrystals: Nonaqueous Synthesis, Growth Mechanism, and Exploitation in Dye-Sensitized Solar Cells. *J. Am. Chem. Soc.* **2011**, *133*, 19216−19239.

(31) Kang, S. H.; Choi, S. H.; Kang, M. S.; Kim, J. Y.; Kim, H. S.; Hyeon, T.; Sung, Y. E. Nanorod-Based Dye-Sensitized Solar Cells with Improved Charge Collection Efficiency. *Adv. Mater.* **2008**, *20*, 54−58.

(32) Li, S.; Li, Y. G.; Wang, H. Z.; Fan, W. G.; Zhang, Q. H. Peptization-Hydrothermal Method as a Surfactant-Free Process Toward Nanorod-Like Anatase TiO_2 Nanocrystals. *Eur. J. Inorg. Chem.* **2009**, *27*, 4078−4084.

(33) Jun, Y. W.; Casula, M. F.; Sim, J. H.; Kim, S. Y.; Cheon, J.; Alivisatos, A. P. Surfactant-Assisted Elimination of a High Energy Facet as a Means of Controlling the Shapes of TiO_2 Nanocrystals. *J. Am. Chem. Soc.* **2003**, *125*, 15981−15985.
(34) Polleux, J.; Pinna, N.; Antonietti, M.; Hess, C.; Wild, U.; Schlogl, R.; Niederberger, M. Ligand Functionality as a Versatile Tool to Control the Assembly Behavior of Preformed Titania Nanocrystals. *Chem.—Eur. J.* **2005**, *11*, 3541−3551.
(35) Niederberger, M.; Colfen, H. Oriented Attachment and Mesocrystals: Non-classical Crystallization Mechanisms Based on Nanoparticle Assembly. *Phys. Chem. Chem. Phys.* **2006**, *8*, 3271−3287.
(36) Jiang, X. C.; Wang, Y. L.; Herricks, T.; Xia, Y. N. Ethylene Glycol-Mediated Synthesis of Metal Oxide Nanowires. *J. Mater. Chem.* **2004**, *14*, 695−703.
(37) Ito, S.; Murakami, T. N.; Comte, P.; Liska, P.; Grätzel, C.; Nazeeruddin, M. K.; Grätzel, M. Fabrication of Thin Film Dye Sensitized Solar Cells with Solar to Electric Power Conversion Efficiency over 10%. *Thin Solid Films* **2008**, *516*, 4613−4619.
(38) Hore, S.; Vetter, C.; Kern, R.; Smit, H.; Hinsch, A. Influence of Scattering Layers on Efficiency of Dye-Sensitized Solar Cells. *Sol. Energy Mater. Sol. Cells* **2006**, *90*, 1176−1188.
(39) Robertson, N. Optimizing Dyes for Dye-Sensitized Solar Cells. *Angew. Chem. Int. Ed.* **2006**, *45*, 2338−2345.
(40) Grätzel, M. Conversion of Sunlight to Electric Power by Nanocrystalline Dye-Sensitized Solar Cells. *J. Photochem. Photobiol., A: Chemistry* **2004**, *164*, 3−14.
(41) Zakeeruddin, S. M.; Nazeeruddin, M. K.; Humphry-Baker, R.; Pechy, P.; Quagliotto, P.; Barolo, C.; Viscardi, G.; Grätzel, M. Design, Synthesis, and Application of Amphiphilic Ruthenium Polypyridyl Photosensitizers in Solar Cells Based on Nanocrystalline TiO_2 Films. *Langmuir* **2002**, *18*, 952−954.
(42) O'Regan, B. C.; Lenzmann, F. Charge Transport and Recombination in a Nanoscale Interpenetrating Network of N-Type and P-Type Semiconductors: Transient Photocurrent and Photovoltage Studies of TiO_2/Dye/CuSCN Photovoltaic Cells. *J. Phys. Chem. B* **2004**, *108*, 4342−4350.
(43) Lagemaat, J. v. d.; Frank, A. J. Nonthermalized Electron Transport in Dye-Sensitized Nanocrystalline TiO2 Films: Transient Photocurrent and Random-Walk Modeling Studies. *J. Phys. Chem. B* **2001**, *105*, 11194−11205.
(44) Nelson, J.; Chandler, R. E. Random Walk Models of Charge Transfer and Transport in Dye Sensitized Systems. *Coord. Chem. Rev.* **2004**, *248*, 1181−1194.
(45) Frank, A. J.; Kopidakis, N.; van de Lagemaat, J. Electrons in Nanostructured TiO_2 Solar Cells: Transport, Recombination and Photovoltaic Properties. *Coord. Chem. Rev.* **2004**, *248*, 1165−1179.
(46) Zhu, K.; Kopidakis, N.; Neale, N. R.; Lagemaat, J. v. d.; Frank, A. J. Influence of Surface Area on Charge Transport and Recombination in Dye-Sensitized TiO_2 Solar Cells. *J. Phys. Chem. B* **2006**, *110*, 25174−25180.
(47) Nakade, S.; Matsuda, M.; Kambe, S.; Saito, Y.; Kitamura, T.; Sakata, T.; Wada, Y.; Mori, H.; Yanagida, S. Dependence of TiO_2 Nanoparticle Preparation Methods and Annealing Temperature on the Efficiency of Dye-Sensitized Solar Cells. *J. Phys. Chem. B* **2002**, *106*, 10004−10010.
(48) Kopidakis, N.; Benkstein, K. D.; Lagemaat, J. v. d.; Frank, A. J. Transport-Limited Recombination of Photocarriers in Dye-Sensitized Nanocrystalline TiO_2 Solar Cells. *J. Phys. Chem. B* **2003**, *107*, 11307−11315.